Accepted Manuscript

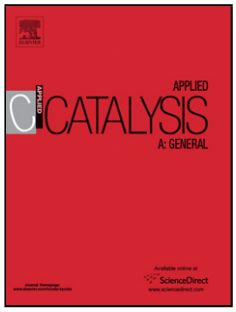


Title: Influence of the catalyst composition in the oxidative dehydrogenation of 1-butene over $BiV_xMo_{1-x}$ oxide catalysts

Author: Jung-Hyun Park Chae-Ho Shin

PII: S0926-860X(15)00068-X
DOI: http://dx.doi.org/doi:10.1016/j.apcata.2014.10.063
Reference: APCATA 15233

To appear in: *Applied Catalysis A: General*

Received date: 28-5-2014
Revised date: 26-8-2014
Accepted date: 5-10-2014

Please cite this article as: J.-H. Park, C.-H. Shin, Influence of the catalyst composition in the oxidative dehydrogenation of 1-butene over $BiV_xMo_{1-x}$ oxide catalysts, *Applied Catalysis A, General* (2015), http://dx.doi.org/10.1016/j.apcata.2014.10.063

This is a PDF file of an unedited manuscript that has been accepted for publication. As a service to our customers we are providing this early version of the manuscript. The manuscript will undergo copyediting, typesetting, and review of the resulting proof before it is published in its final form. Please note that during the production process errors may be discovered which could affect the content, and all legal disclaimers that apply to the journal pertain.

ACCEPTED MANUSCRIPT

# Influence of the catalyst composition in the oxidative dehydrogenation of 1-butene over $BiV_xMo_{1-x}$ oxide catalysts

Jung-Hyun Park, Chae-Ho Shin†

*Department of Chemical Engineering, Chungbuk National University, 361-763 Cheongju, Korea*

Accepted Manuscript

*Highlights*

ACCEPTED MANUSCRIPT

- ►Effect of catalyst composition on $BiV_xMo_{1-x}$ oxide catalyst was investigated.
- ►The catalyst composition affects remarkably the conversion and selectivity.
- ►$BiV_{0.6}Mo_{0.4}$ catalyst shows an excellent activity for oxidative dehydrogenation.
- ►Yield in 1,3-butadiene is correlated with the oxygen mobility.

†To whom correspondence should be addressed.

E-mail: chshin@chungbuk.ac.kr

**Abstract**

$BiV_xMo_{1-x}$ oxide catalysts with varying compositions were investigated in the oxidative dehydrogenation (ODH) of 1-butene to 1,3-butadiene (BD). Notably, incorporation of vanadium in the Bi-Mo oxide significantly enhanced the catalytic performance in the ODH of 1-butene. Among the tested catalysts, the $BiV_{0.6}Mo_{0.4}$ oxide catalyst exhibited superior oxygen mobility in temperature-programmed re-oxidation experiments, revealed the facile desorption of adsorbed BD species in the temperature-programmed desorption of 1-butene,



Accepted Manuscript

ACCEPTED MANUSCRIPT

and displayed the highest performance (72.2% conversion of 1-butene and 64.0% yield in BD) in the ODH of 1-butene. Moreover, the performance of the tested catalysts decreased in the following order $BiV_{0.6}Mo_{0.4}$ > $BiV_{0.4}Mo_{0.6}$ > $BiV_{0.8}Mo_{0.2}$ > $BiV_{0.2}Mo_{0.8}$ > BiMo > BiV. In addition, the $BiV_{0.6}Mo_{0.4}$ oxide catalyst displayed stable performance over 85 h and its excellent catalytic ability makes it economically viable.

Keywords

$BiV_xMo_{1-x}$ oxide catalyst

Catalyst composition

1,3-butadiene

Temperature-programmed re-oxidation

Oxygen mobility

Accepted Manuscript

ACCEPTED MANUSCRIPT

## 1. Introduction

1,3-butadiene (BD) constitutes an important raw material for the production of compounds such as styrene butadiene rubber (SBR), poly-butadiene rubber (BR), and acrylonitrile-butadiene-styrene resin (ABS) [1]. Over 98% of the global BD supply is produced by extracting C4 raffinates from naphtha cracking. However, the generated BD supply from this process does not satisfy the demands of the petrochemical market. Therefore, alternative methods are required for the efficient production of BD. Of the available alternatives, the oxidative dehydrogenation (ODH) of *n*-butenes has received significant attention, because this reaction can produce BD in a high yield [2,3]. Various metal oxide catalysts such as manganese oxide molecular sieves [4], K-doped $VO_x/Al_2O_3$ [5], ferrite catalysts [6,7], and pure bismuth-molybdate catalysts or bismuth-molybdate based multicomponent oxide catalysts [8-17] have been tested in the ODH of *n*-butenes. Among these catalysts, bismuth-molybdate-based catalysts have been studied intensively. In particular, multicomponent oxide catalysts composed of various transition metals and non-metals have been widely investigated in an attempt to improve the low catalytic performance of pure bismuth-molybdate catalysts [8-17]. In previous works, we compared the catalytic performance of multicomponent Bi-Fe-Me(x)-Mo oxide catalysts prepared by the addition of different transition metals. Notably, $BiFe_{0.65}Ni_{0.05}Mo$ oxide exhibited the best catalytic performance in the ODH of 1-butene [11]. Jung et al. reported that $Co_9Fe_3Bi_1Mo_{12}O_{51}$ showed the highest oxygen mobility and the best catalytic performance in the ODH of *n*-butenes [13].

Vanadium oxide is an effective catalyst or promoter of selective oxidation to

ACCEPTED MANUSCRIPT

yield acrolein from propylene and from *n*-butenes to butadiene [18-21]. Rossi et al. [22] reported the catalytic performance of a scheelite-structured catalyst containing vanadium in the ODH of 1-butene. Notably, the cationic vacancy of the catalysts facilitated allylic oxidation and lattice oxygen diffusion. Ueda et al. [23] reported that in the oxidation of propylene, the catalytic performance of $Bi_{1-x/3}V_{1-x}Mo_xO_4$ with a scheelite-like structure increased upon substitution of $V^{5+}$ ions with $Mo^{6+}$ ions, without any concomitant changes in the selectivity towards acrolein.

The ODH of *n*-butenes occurs via three major elementary steps according to the Mars-van Krevelen (MvK) mechanism [24]. First, the alkene is adsorbed on the catalyst surface and is activated by the abstraction of the α hydrogen to the double bond to produce an allylic intermediate. Next, the catalyst' oxygen is inserted into the activated allylic intermediate and the intermediate reacts via the lattice oxygen to form the desired products. Finally, the reduced catalyst is oxidized by a supply of gaseous oxygen. The oxygen mobility of the catalyst is critical to the catalytic activity in ODH reactions, and many researchers have measured this property using various analytical tools such as temperature programmed re-oxidation [9-11,25], temperature-programmed desorption of $O_2$ [26,27], and $^{18}O/^{16}O$ isotopic exchange measurements [28], etc. In previous works, we performed temperature programmed re-oxidation measurements to determine the oxygen mobility of certain catalysts and found that catalysts with high oxygen mobility exhibited superior performance in the ODH of 1-butene [9-11].

Here, the catalytic performance of $BiV_xMo_{1-x}$ oxide catalysts with different V/Mo molar ratios (x = 0-1.00; Bi to V/Mo molar ratio was set at 1.0), prepared by co-

ACCEPTED MANUSCRIPT

precipitation, were evaluated in the ODH of 1-butene to BD. $BiV_xMo_{1-x}$ oxide catalysts were characterized using X-ray diffraction (XRD), $N_2$ sorption, Raman spectroscopy, Inductively coupled plasma atomic emission spectroscopy (ICP-AES), 1-butene temperature-programmed desorption (1-butene TPD) and temperature-programmed re-oxidation (TPRO).

## 2. Experimental

### *2.1. Catalyst preparation*

A series of $BiV_xMo_{1-x}$ oxide catalysts (x = 0.0-1.0) was prepared by co-precipitation. Bismuth nitrate ($Bi(NO_3)_3{\cdot}5H_2O$, Junsei, 98%), ammonium heptamolybdate ($(NH_4)_6Mo_7O_{24}{\cdot}4H_2O$, Junsei, 99%), and ammonium metavanadate ($NH_4VO_3$, Sigma-aldrich, 99%) were used as received without further purification. Mixed metal oxide samples were prepared according to the following procedure: bismuth nitrate was dissolved in deionized water acidified with 10% nitric acid. Ammonium metavanadate and ammonium heptamolybdate were dissolved in deionized water at 70 $^oC$, respectively. To prepare the mixed metal solution, the vanadium- and bismuth-containing solutions were added to the molybdenum-containing solution with vigorous stirring at 70 $^oC$ and the pH of the mixed metal solution was adjusted to 8 using $NH_4OH$ (Samchun, 28-30 vol%). The resulting solution was vigorously stirred at





Accepted Manuscript

ACCEPTED MANUSCRIPT

70 $^{o}$C for 1 h and was then filtered and washed several times with deionized water. The solid product was dried at 100 $^{o}$C for 12 h and calcined at 550 $^{o}$C for 2 h under a flow of air.

*2.2. Characterization*

The crystalline structures of the $BiV_xMo_{1-x}$ oxide catalysts were recorded on an X-ray diffractometer (Bruker D5005) using CuKα radiation (30 kV and 50 mA) with a scan rate of 1.2$^{o}$ min$^{-1}$. The XRD phases of the $BiV_xMo_{1-x}$ oxide catalysts were identified by their characteristic diffraction peaks using JCPDS files. The surface areas and pore volumes of the catalysts were determined by $N_2$ adsorption at -196 $^{o}$C using a Micromeritics ASAP 2020. Prior to the measurement, 0.5g of the sample was degassed at 250 $^{o}$C for 4 h. The surface area was determined using the Brunauer-Emmett-Teller (BET) equation in the range of $P/P_o$ = 0.05-0.20 and the total pore volume was measured at $P/P_o$ = 0.99.

Elemental analysis was carried out using inductively coupled plasma atomic emission spectroscopy (ICP-AES, Jarrell-Ash Polyscan 61E) in combination with a Perkin-Elmer 5000 atomic absorption spectrophotometer. Scanning electron microscopy (SEM) images of the catalysts were acquired on a Hitachi S-2500C scanning electron microscope at an acceleration voltage of 5 kV. Raman spectra were recorded on a Bruker Optic GMBH FRA 106/S with an Nd:YAG laser (300 mW, 500 scans).

Temperature-programmed re-oxidation (TPRO) was performed in a U-shaped





Accepted Manuscript

ACCEPTED MANUSCRIPT

quartz reactor, and 0.15 g of the catalyst was used for each measurement in order to elucidate the oxygen mobility. Prior to the analysis, the catalysts were pretreated at 420 $^{o}$C for 1 h with a mixture of 50% $H_2$ in Ar (100 $cm^3$ $min^{-1}$) and were then cooled to room temperature (RT) under the same atmosphere. In this step, the catalysts would be reduced by the $H_2$-Ar flow. To confirm the degree of oxygen consumption by the oxidation reaction occurring on the reduced sites of the catalysts, a flow of 5% $O_2$ in $N_2$ (20 $cm^3$ $min^{-1}$) was utilized in the reactor and the catalyst was subsequently heated to 600 $^{o}$C from RT at a heating rate of 10 $^{o}$C $min^{-1}$. The mass signal of $m/z$ = 32 ($\cdot O_2$) in the outlet gas was measured by mass spectroscopy (MS, Pfeiffer vacuum QMS 200).

$O_2$-pulse experiments were performed using the same apparatus as that used for TPRO in order to measure the quantity of oxygen consumed during catalyst re-oxidation. Prior to the analysis, 0.15 g samples were reacted at 420 $^{o}$C for 1 h under the specified reaction conditions and were flushed for 1 h with a 30 $cm^3$ $min^{-1}$ Ar flow. To measure the oxygen consumption of the reduced catalyst sites, 71.0 μmol of $O_2$ with an Ar carrier (2 $cm^3$ sample loop) was introduced into the catalyst bed every 5 min and pulse experiments were repeated 8 times. The mass signal of $m/z$ = 32 ($\cdot O_2$) in the outlet gas was measured using the same MS analyzer as that in the TPRO experiments.

In order to elucidate the adsorption-desorption behavior of 1-butene, temperature-programmed desorption of 1-butene (1-butene TPD) was carried out using a similar apparatus to that in the TPRO measurements. Prior to the analysis, the catalysts were pretreated at 200 $^{o}$C for 1 h with Ar (30 $cm^3$ $min^{-1}$) and then cooled to RT. The catalyst was then treated at RT for 0.5 h with 1-$C_4H_8$ (20 $cm^3$ $min^{-1}$). Following the adsorption of 1-butene at RT, the sample was purged under a flow of Ar (30 $cm^3 \cdot min^{-1}$)





Accepted Manuscript

ACCEPTED MANUSCRIPT

for 0.5 h. TPD was performed from 50 to 800 $^{o}$C at a heating rate of 10 $^{o}$C min$^{-1}$. The mass signals of *m/z* = 18 ($\cdot H_2O$), 44 ($\cdot CO_2$), and 54 ($\cdot C_4H_6$) were detected using the same MS analyzer as that used in the TPRO experiments.

*2.3. Catalytic testing*

The ODH of 1-butene was carried out at ambient pressure with 0.5 g of the catalyst in a continuous flow fixed-bed reactor. Prior to the reaction, all catalysts were pretreated at 500 $^{o}$C for 2 h with a flow of $N_2$ (50 cm$^3$ min$^{-1}$) and were cooled to 420 $^{o}$C under the same atmosphere. The feed composition was fixed at 1-$C_4H_8$/air/steam = 1/3.75/5 with a total flow rate of 78 cm$^3$ min$^{-1}$. Steam was sufficiently vaporized by passage through an evaporator. The products were analyzed by an on-line gas chromatograph (Varian 3800) with an $Al_2O_3$/KCl column (FID detector) for hydrocarbons and a Porapak Q packed column (TCD detector) for CO and $CO_2$. The production of CO was negligible under the reaction conditions. Cracking products such as $CH_4$, $C_2H_6$, and $C_3H_8$ were minor or negligible. The conversion, selectivity and yield in BD were calculated following previously reported procedures [29].

## 3. Results and discussion

*3.1. Characterization of catalysts*



Accepted Manuscript

ACCEPTED MANUSCRIPT

Fig. 1 shows the XRD patterns of the $BiV_xMo_{1-x}$ oxide catalysts prepared with different V/Mo molar ratios. Generally, BiMo oxide is composed of three phases, α-$Bi_2Mo_3O_{12}$, β-$Bi_2Mo_2O_9$, and γ-$Bi_2Mo_1O_6$. β-$Bi_2Mo_2O_9$ partially decomposed to α-$Bi_2Mo_3O_{12}$ and γ-$Bi_2Mo_1O_6$ due to the calcination temperature [9,30]. BiMo oxide with Bi/Mo = 1.0 calcined at 550 $^oC$ contained two mixed phases, namely, γ-$Bi_2Mo_1O_6$, and β-$Bi_2Mo_2O_9$. The BiV oxide catalyst showed the typical $BiVO_4$ phase. The $BiV_xMo_{1-x}$ oxide catalysts exhibited different phases according to their composition. Catalysts with high vanadium contents ($BiV_{0.8}Mo_{0.2}$, $BiV_{0.6}Mo_{0.4}$, and $BiV_{0.4}Mo_{0.6}$), displayed $Bi_{0.93}Mo_{0.21}V_{0.79}O_4$ and $Bi_{0.93}Mo_{0.37}V_{0.63}O_4$ with a minor phase of γ-$Bi_2Mo_1O_6$, respectively, while the catalyst with a low vanadium content ($BiV_{0.2}Mo_{0.8}$) crystallized primarily in the γ-$Bi_2Mo_1O_6$ phase (Table 1). The relative intensities of the constituent phases in the $BiV_xMo_{1-x}$ oxide catalysts were also different depending on the molar ratio of V/Mo. In addition, the diffraction patterns of the $BiV_xMo_{1-x}$ oxide catalysts shifted to a higher angle with decreasing Mo contents. Since the radii of $V^{5+}$ cations (0.068 nm) are smaller than those of $Mo^{6+}$ cations (0.073 nm), $V^{5+}$ cations can be inserted into the BiMo oxide catalyst [31], which leads to the formation of solid solution phases.

The BET surface areas and the total pore volumes of the $BiV_xMo_{1-x}$ oxide catalysts are listed in Table 1. The BET surface areas of the $BiV_xMo_{1-x}$ oxide catalysts were smaller than those of the pure BiMo oxide catalysts (3.9 $m^2\ g^{-1}$), but, larger than that of the BiV oxide catalyst (0.9 $m^2\ g^{-1}$). The BET surface areas of the $BiV_xMo_{1-x}$ oxide catalysts showed no significant changes upon variation of the vanadium content (2.6-4.6 $m^2\ g^{-1}$). The atomic ratios of the metal components are also summarized in





Accepted Manuscript

ACCEPTED MANUSCRIPT

Table 1. The catalyst composition was calculated as the molar ratio of each metal component with respect to that of Bi. The catalyst molar ratios determined by ICP-AES analysis were nearly consistent with the molar ratio of the mother solution, and were in relatively good agreement with the theoretical values, suggesting that the $BiV_xMo_{1-x}$ oxide catalysts were successfully prepared.

Fig. 2 shows the SEM images of the $BiV_xMo_{1-x}$ oxide catalysts with varying compositions. The morphology and particle size of the $BiV_xMo_{1-x}$ oxide catalysts greatly depended on the composition. BiMo oxide exhibited nanostructures with diameters ranging between 100 and 200 nm. $BiV_{0.2}Mo_{0.8}$, $BiV_{0.4}Mo_{0.6}$, and $BiV_{0.6}Mo_{0.4}$ oxide catalysts showed somewhat different particle shapes as compared to the BiMo oxide catalyst (Fig. 2(b-d)). In addition, the particle sizes of the $BiV_xMo_{1-x}$ oxide catalysts were larger than that of the BiMo oxide catalyst. The particle sizes of the vanadium-rich catalysts ($BiV_{0.8}Mo_{0.2}$, and BiV) were significantly greater than those of other catalysts (≈10 μm), and the morphology of the catalysts was nearly spherical and consisted of small microspheres. A similar observation was reported previously [32].

Raman spectroscopy can provide structural information and is a sensitive method for the investigation of local structure and electronic properties of various samples. Fig. 3 shows the Raman spectra of the $BiV_xMo_{1-x}$ oxide catalysts with different V/Mo molar ratios. Vibrational bands of the BiV oxide catalyst were observed at 212, 325, 367, and 828 $cm^{-1}$. These bands corresponded to the typical vibrational bands of $BiVO_4$ [33,34]. The band at 828 $cm^{-1}$ was assigned to the symmetric V-O stretching mode, while the peaks at 325 and 367 $cm^{-1}$ were assigned to the asymmetric and symmetric bending vibration of the $VO_4$ tetrahedron. The band at 212 $cm^{-1}$ represented





Accepted Manuscript

ACCEPTED MANUSCRIPT

the external vibrations [34,35]. The vibrational bands of the BiMo oxide catalyst were observed around 284, 293, 354, 404, 715, 780, 807, and 852 $cm^{-1}$, corresponding to the typical vibrational bands of γ-$Bi_2Mo_1O_6$ [36,37]. For catalysts with high vanadium contents ($BiV_{0.8}Mo_{0.2}$, $BiV_{0.6}Mo_{0.4}$, and $BiV_{0.4}Mo_{0.6}$), the mixed oxides showed similar Raman spectra. The vibrational bands at 336, 817, 880, and 883 $cm^{-1}$ were assigned to the Bi-V-Mo mixed phase. The peak shift was speculated to be related to the catalyst composition. In addition, vibrational bands related to γ-$Bi_2Mo_1O_6$ were also observed in all $BiV_xMo_{1-x}$ oxide catalysts. For the catalyst with a low vanadium content ($BiV_{0.2}Mo_{0.8}$), the spectrum was very similar to that of the BiMo oxide catalyst. Overall, the Raman results were in good agreement with the XRD results.

*3.2. Catalytic testing*

Fig. 4 shows the catalytic performance of the $BiV_xMo_{1-x}$ oxide catalysts in the ODH of 1-butene to BD after an 8 h reaction, plotted as a function of the vanadium content. For all catalysts, BD and $CO_2$ constituted the main products and small amounts of cracking products, such as $CH_4$, and $C_2H_6$ were also observed. All catalysts showed stable catalytic performance over 8 h on stream (Fig. S1 in the supplementary data). Notably, the catalyst composition had a significant influence on the catalytic performance of the $BiV_xMo_{1-x}$ oxide catalysts. The conversion of 1-butene and yield in BD were maximized at a vanadium content of x = 0.6. The selectivity toward BD increased, whereas the selectivity towards $CO_2$ decreased with respect to the vanadium

ACCEPTED MANUSCRIPT

content and showed a reverse volcano-shaped curve with respect to the vanadium content. The conversion of 1-butene and the yield in BD with the $BiV_{0.6}Mo_{0.4}$ oxide catalyst were 72.2% and 64.0%, respectively. The catalytic performance of the catalysts in the ODH of 1-butene decreased in the following order: $BiV_{0.6}Mo_{0.4}$ > $BiV_{0.4}Mo_{0.6}$ > $BiV_{0.8}Mo_{0.2}$ > $BiV_{0.2}Mo_{0.8}$ > BiMo > BiV. Table S1 lists the catalytic performance of the reported catalysts in the ODH reaction. The catalytic performance of the catalysts used in this study was slightly lower than those reported previously. Further studies are required in order to improve the catalytic performance of BiVMo oxide catalytic systems.

*3.3. TPRO*

In order to elucidate the oxygen mobility of the $BiV_xMo_{1-x}$ oxide catalysts, TPRO analysis was performed with the reduced catalysts, as shown in Fig. 5 (A). It is well known that the oxygen mobility of the catalysts is important in the ODH of butenes. The peak temperatures observed during TPRO runs reflect the oxygen mobility of the catalysts, in that lower desorption peak temperatures reveal a higher oxygen mobility [9,40,41]. For the $BiV_xMo_{1-x}$ oxide catalysts, several oxidation peaks were observed for each catalyst. The first peak in the 150-250 $^oC$ range was a sharp and asymmetric peak. The other peaks appeared in the 280-500 $^oC$ range and were related to the oxidation of the partially reduced bismuth and molybdenum species [42]. The first peak was shifted to lower temperatures with increasing vanadium content, and the minimum value was

ACCEPTED MANUSCRIPT

observed with the $BiV_{0.6}Mo_{0.4}$ oxide catalyst. The peak position sequence of the other catalyst was in the following order: $BiV_{0.6}Mo_{0.4}$ < $BiV_{0.4}Mo_{0.6}$ < $BiV_{0.8}Mo_{0.2}$ < $BiV_{0.2}Mo_{0.8}$ < BiMo < BiV. This was in good agreement with the catalytic performance of the catalysts.

Fig. 5 (B) shows the correlation between the yield in BD and the oxygen mobility of the $BiV_xMo_{1-x}$ oxide catalysts. The yield in BD increased with lower TPRO temperatures. The $BiV_{0.6}Mo_{0.4}$ catalyst showed the lowest TPRO peak temperature (181 $^oC$), while the BiV oxide catalyst showed the highest TPRO peak temperature (254 $^oC$). The $BiV_{0.6}Mo_{0.4}$ oxide catalyst, which showed the lowest TPRO peak temperature, exhibited the best catalytic performance among the catalysts. As such, high catalytic performance can be attributed to the oxygen mobility of the catalyst. In order to measure the quantity of oxygen consumed, $O_2$-pulse experiments were carried out and the results are shown in Table 1. In the $O_2$-pulse experiments, the introduced oxygen was completely consumed during the 3 pulses and subsequently, distinct changes were not observed (Fig. S2), indicating that the reduced catalyst was completely re-oxidized. The consumed oxygen was related to the oxygen migration to the catalyst surface or lattice and was calculated by integrating the detected $O_2$ peak during the $O_2$-pulse experiments. The total quantity of consumed oxygen on $BiV_{0.6}Mo_{0.4}$ oxide was much larger than that on the other catalysts (Table 1). The oxygen consumption decreased in the following order: $BiV_{0.6}Mo_{0.4}$ > $BiV_{0.4}Mo_{0.6}$ > $BiV_{0.8}Mo_{0.2}$ > $BiV_{0.2}Mo_{0.8}$ > BiMo > BiV, and was in good agreement with the catalytic performance; however, there was no direct correlation between the quantity of consumed $O_2$ and BD selectivity.

ACCEPTED MANUSCRIPT

*3.4. TPD of 1-butene*

TPD analysis was performed to investigate the desorption characteristics of 1-butene over the $BiV_xMo_{1-x}$ oxide catalysts. The TPD patterns of 1-butene are shown in Fig. 6 and 7, where the response of *m/z* = 54 ($\cdot C_4H_6$) was plotted as a functions of desorption temperature. BD ($\cdot C_4H_6$) is the product of 1-butene with lattice or surface oxygen in the $BiV_xMo_{1-x}$ oxide catalysts. The TPD profiles of *m/z* = 56 ($\cdot C_4H_8$) gradually decreased with increasing desorption temperature until 450 $^oC$. Above this temperature, no desorption of 1-butene was observed. Furthermore, $H_2O$ and $CO_2$, the products of 1-butene with non-selective oxygen at the combustion sites, were completely desorbed above 500 $^oC$ (Fig. 6). The TPD profiles of all $BiV_xMo_{1-x}$ oxide catalysts revealed a broad and asymmetric peak. The peak temperature showed a diminishing trend with respect to the vanadium content, indicating that the desorption of BD was influenced by the vanadium content. In addition, the quantity of desorbed BD increased with increasing vanadium content, and showed a maximum value at x = 0.6 in $BiV_xMo_{1-x}$ oxide.

Fig. 7(B) depicts the correlation between the catalytic performance and the quantity of desorbed BD and desorption temperature. The quantity of BD obtained via integration of the TPD profile exhibited a volcano-shaped curve with respect to the vanadium content, and the $BiV_{0.6}Mo_{0.4}$ oxide catalyst yielded the largest quantity of BD as compared to the other catalysts, indicating that the $BiV_{0.6}Mo_{0.4}$ oxide catalyst had more lattice/surface oxygen or adsorption sites. Also, the desorption temperature of BD resulted in a reverse-volcano shaped curve with respect to the vanadium content, and the

ACCEPTED MANUSCRIPT

$BiV_{0.6}Mo_{0.4}$ oxide catalyst presented the lowest desorption temperature, indicating that the BD adsorbed on the $BiV_{0.6}Mo_{0.4}$ oxide catalyst was more easily desorbed as compared to on the other catalysts. From the TPD analysis, it can be concluded that the catalytic performance was closely related to the quantity of lattice/surface oxygen, adsorption sites, and facile desorption of BD.

Fig. 3S shows the MS signals in the reaction over the $BiV_{0.6}Mo_{0.4}$ oxide catalyst in the absence of an oxygen feed. All other reaction parameters were fixed as the standard reaction conditions. Under the $O_2$-free reaction conditions, the MS signal of $\cdot C_4H_8$ (*m/z* = 56) slightly decreased at the beginning of reaction and subsequently exhibited a constant value. The MS signals of $\cdot CO_2$ (*m/z* = 44) and $\cdot C_4H_6$ (*m/z* = 54) gradually decreased as a function of time and finally reached zero after 35 min. This indicates that the $BiV_{0.6}Mo_{0.4}$ oxide catalyst consumed lattice oxygen during the reaction in the absence of an oxygen feed, which is in good agreement with the MvK mechanism and is been generally accepted in the ODH of butenes [10,26,40]. Therefore, the peak area of the BD signal reflects the quantity of lattice oxygen, which can be calculated by integrating the peak area. The reduced catalyst upon reaction with 1-$C_4H_8$ can be re-oxidized via a supply of gas phase oxygen. Facile reduction-oxidation cycles are critical in enhancing the catalytic performance.

*3.5. Long-term stability test*

To assess the stability of the catalyst, a long-term stability test of the $BiV_{0.6}Mo_{0.4}$

ACCEPTED MANUSCRIPT

oxide catalyst was carried out and the results are shown in Fig. 8. Conversion of 1-butene was maintained throughout the reaction. The selectivity towards BD gradually increased and the selectivity towards $CO_2$ decreased over 30 h. After 30 h, the selectivities towards the products were maintained. The conversion of 1-butene and the yield in BD after 85 h were 72.5%, and 64.0%, respectively. The $BiV_{0.6}Mo_{0.4}$ oxide catalyst showed suitable catalytic performance and stability, rendering it economically viable.

## 4. Conclusions

$BiV_xMo_{1-x}$ oxide catalysts with various vanadium contents (x = 0-1.0) were prepared and their performance in the ODH of 1-butene to BD was evaluated. The formation of the $BiV_xMo_{1-x}$ oxide catalysts was confirmed via XRD and ICP analysis. The catalytic performance in the ODH reaction of 1-butene depended on the catalyst composition. The oxygen mobility of the $BiV_xMo_{1-x}$ oxide catalysts was related to their catalytic performance. The $BiV_{0.6}Mo_{0.4}$ oxide catalyst, which gave the best catalytic performance, showed the lowest TPRO temperature. The $BiV_{0.6}Mo_{0.4}$ oxide catalyst displayed the highest catalytic performance and stability during long-term stability tests.

## Acknowledgement



Accepted Manuscript

ACCEPTED MANUSCRIPT

This work was financially supported by the Industrial Strategic technology development program (2014-10042591) funded by the Ministry of Trade, industry & Energy (MOTIE, Korea).

## References

[1] W.C. White, Chem. Biol. Interact. 166 (2007) 10–14.

[2] H.H. Voge, C.R. Adams, Adv. Catal. 17 (1967) 151–221.

[3] H.H. Kung, Eng. Chem. Prod. Res. Dev. 25 (1986) 171–178

[4] V.V. Krishnan, S.L. Suib, J. Catal. 184 (1999) 305–315.

[5] J.M.L. Nieto, P. Concepcion, A. Dejoz, F. Melo, H. Knozinger, M.I. Vazquez, Catal. Today 61 (2000) 361–367.

[6] J.A. Toledo-Antonio, N. Nava, M. Martinez, X. Bokhimi, Appl. Catal. A: Gen. 234 (2002) 137–144.

[7] H.W. Lee, J.C. Jung, H.S. Kim, Y.M. Chung, T.J. Kim, S.J. Lee, S.H. Oh, Y.S. Kim, I.K. Song, Catal. Lett. 122 (2008) 281–286.

[8] J.C. Jung, H.W. Lee, S.Y. Park, Y.-M. Chung, T.J. Kim, S.J. Lee, S.-H. Oh, Y.S. Kim, I.K. Song, Korean J. Chem. Eng. 25 (2008) 1316–1321.

[9] J.-H. Park, H.R. Noh, J. W. Park, K.H. Row, K. D. Jung, C.-H. Shin, Appl. Catal. A: Gen. 431-432 (2012) 137–143.

[10] J.-H. Park, K.H. Row, C.-H. Shin, Catal. Commun. 31 (2013) 76–80.

[11] J.-H. Park, C.-H. Shin, J. Ind. Eng. Chem. (2014) DOI:10.1016/j.jiec.2014.03.037.



Accepted Manuscript

ACCEPTED MANUSCRIPT

[12] Y. Moro-Oka, W. Ueda, Adv. Catal. 40 (1994) 233–273.

[13] J.C. Jung, H.W. Lee, J.G. Seo, S.Y. Park, Y.-M. Chung, T.J. Kim, S.J. Lee, S.-H. Oh, Y.S. Kim, I.K. Song, Catal. Today 141 (2009) 325–329.

[14] J.F. Brazdil, D. D. Suresh, R.K. Grasselli, J. Catal. 66 (1980) 347–367.

[15] M.W.J. Wolfs, P.H.A. Batist, J. Catal. 32 (1974) 25–36.

[16] J.M.M. Millet, H. Ponceblanc, G. Coudurier, J.M. Herrmann, J.C. Vedrine, J. Catal. 142 (1993) 381–391.

[17] V. Fattore, Z.A. Fuhrman, G. Manara, B. Notari, J. Catal. 37 (1975) 223–231.

[18] N.F. Dummer, J. K. Bartley, G. J. Hutchings, Adv. Catal. 54 (2011) 189–247.

[19] T. Seiyama, K. Nita, T. Maehara, N. Yamazoe, Y. Takita, J. Catal. 49 (1977) 164–173.

[20] L.Y. Margolis, Adv. Catal. 14 (1963) 429–501.

[21] M.A. Pepera, J.L. Callahan, M.J. Desmond, E.C. Milberger, P.R. Blum, N.J. Mremer, J. Am. Chem. Soc. 107 (1985) 4883–4892.

[22] S.D. Rossi, M.L. Jacono, M. Gardini, P. Porta, J. Catal. 146 (1994) 126–135.

[23] W. Ueda, K. Asakawa, C.-L. Chen, Y. Moro-oka, T. Ikawa, J. Catal. 101 (1986) 360–368.

[24] R.K. Grasselli, J.D. Burrington, Adv. Catal. 30 (1981) 133–163.

[25] J. K. Lee, H.W. Lee, U. G. Hong, J.S. Lee, Y.-J. Cho, Y.S. Yoo, H.-S. Jang, I. K. Song, J. Ind. Eng. Chem. 18 (2012) 1096–1101.

[26] J.C. Jung, H.W. Lee, H.S. Kim, Y.-M. Chung, T. J. Kim, S.J. Lee, S.-H. Oh, Y.S. Kim, I.K. Song, Catal. Commun. 9 (2008) 943–949.

[27] J.P. Jolya, C. MeÂhier, K.E. BeÂreÂ, M. Abon, Appl. Catal. A: Gen. 169 (1998) 55–63.



Accepted Manuscript

ACCEPTED MANUSCRIPT

[28] I. Brown, W.R. Patterso, J. Chem. Soc. Faraday Trans, 79 (1983) 1431–1449.

[29] J.-H. Park, H.R. Noh, J.W. Park, K.H. Row, K.D. Jung, C.-H. Shin, Res. Chem. Intermed. 37 (2011) 1125–1134.

[30] J.C. Jung, H.S. Kim, Y.-M. Chung, T. J. Kim, S.J. Lee, S.-H. Oh, Y.S. Kim, I.K. Song, J. Mol. Catal. A 264 (2007) 237–240.

[31] http://en.wikipedia.org/wiki/Ionic_radius.

[32] W. Yin, W. Wang, L. Zhou, S. Sun, L. Zhang, J. Hazard. Mater. 173 (2010) 194–199.

[33] T. Yang, D.G. Xia, G. Chen, Y. Chen, Mater. Chem. Phys. 114 (2009) 69–72.

[34] J. Yu, Y. Zhang, A. Kudo, J. Solid State Chem. 182 (2009) 223–228.

[35] S.-I. Eda, M. Fujishima, H. Tada, Appl. Catal. B: Environ. 125 (2012) 288–293.

[36] J.C. Jung, H.W. Lee, I.K. Song, Catal. Surv. Asia 13 (2009) 78–93.

[37] E.V. Hoefs, J.R. Monnier, G. W. Keulks, J. Catal. 57 (1979) 331–337.

[38] W.Yan, Q.Y. Kouk, J. Luo, Y. Liu, A. Borgna, Catal. Commun. 46 (2014) 208–212.

[39] X.Liu, D. S. Su, R. Schlögl, Carbon 46 (2008) 547–549.

[40] L.T. Weng, B. Delmon, Appl. Catal. A: Gen. 81 (1992) 141–213.

[41] H.F. Christmann, US Patent, 3,270,080 (1966).

[42] H. Miura, Y. Morikawa, T. Shirasaki, J. Catal. 39 (1975) 22–28.

ACCEPTED MANUSCRIPT

## Graphical Abstract

# Influence of the catalyst composition in the oxidative dehydrogenation of 1-butene over $BiV_xMo_{1-x}$ oxide catalysts

Jung-Hyun Park, Chae-Ho Shin*

*Department of Chemical Engineering, Chungbuk National University,Chungbuk 361-763, Korea*

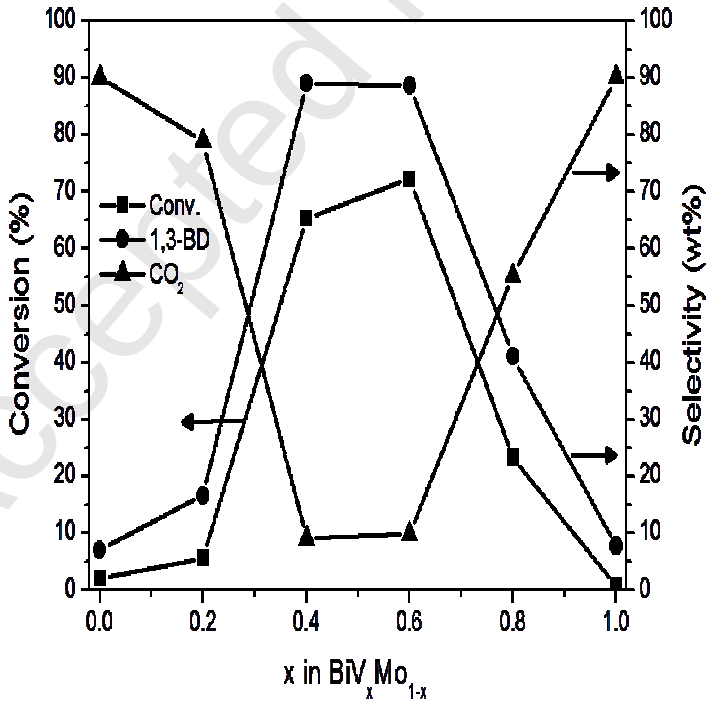


Conversion of 1-butene and selectivity to 1,3-butadiene and $CO_2$ with respect to V/Mo molar ratios



Accepted Manuscript

ACCEPTED MANUSCRIPT

* Corresponding author. Tel.: +82-43-261-2376; fax: 82-43-269-2370.

*E-mail address*: chshin@chungbuk.ac.kr (C.-H. Shin).

Accepted Manuscript

ACCEPTED MANUSCRIPT

**Figure captions**

Fig. 1 XRD patterns of $BiV_xMo_{1-x}$ oxide catalysts: (a) BiMo, (b) x = 0.2, (c) 0.4, (d) 0.6, (e) 0.8, and (f) BiV.

Fig. 2 SEM images of $BiV_xMo_{1-x}$ oxide catalysts: (a) BiMo, (b) x = 0.2, (c) 0.4, (d) 0.6, (e) 0.8, and (f) BiV.

Fig. 3 Raman spectra of $BiV_xMo_{1-x}$ oxide catalysts: (a) BiMo, (b) x = 0.2, (c) 0.4, (d) 0.6, (e) 0.8, and (f) BiV.

Fig. 4 Catalytic activity over $BiV_xMo_{1-x}$ oxide catalyst in the ODH after an 8 h reaction. Reaction conditions: 0.5 g catalyst, T = 420 $^oC$, 1-$C_4H_8$/air/$H_2O$ = 1/3.75/5 and total flow rate of 78 $cm^3$ $min^{-1}$.

Fig. 5 (A) TPRO profiles of reduced $BiV_xMo_{1-x}$ oxide catalysts and (B) correlation curve between the yield in BD and the TPRO peak temperature: (a) BiMo, (b) x = 0.2, (c) 0.4, (d) 0.6, (e) 0.8, and (f) BiV.

Fig. 6 MS signals of 1-butene TPD of $BiV_{0.4}Mo_{0.6}$ oxide catalyst.



Accepted Manuscript

ACCEPTED MANUSCRIPT

Fig. 7 (A) 1-Butene-TPD profiles of $BiV_xMo_{1-x}$ oxide catalysts and (B) correlation curve between the peak area, temperature, and catalyst composition: (a) BiMo, (b) x = 0.2, (c) 0.4, (d) 0.6, (e) 0.8, and (f) BiV.

Fig. 8 Long-term stability test over $BiV_{0.6}Mo_{0.4}$ oxide catalyst in the ODH: (a) conversion and yield in BD and (b) selectivity towards BD and $CO_2$.

Accepted Manuscript

ACCEPTED MANUSCRIPT

**Table 1** physicochemical property of the $BiV_xMo_{1-x}$ oxide catalysts and their catalytic performance

| Catalyst | $S_{BET}$ ($m^2$ $g^{-1}$) | XRD phase | Oxygen quantity (μmol)[a] | Composition (mol)[b] | | | Catalytic performance[c] | | | |
|---|---|---|---|---|---|---|---|---|---|---|
| | | | | | | | Conv. | Selectivity (wt.%) | | Yield |
| | | | | Bi | V | Mo | (%) | BD | $CO_2$ | (wt.%) |
| BiMo | 3.9 | γ-$Bi_2Mo_1O_6$, β-$Bi_2Mo_2O_9$ | 103.3 | 1.00 | - | 0.85 | 2.0 | 7.0 | 90.1 | 0.1 |
| $BiV_{0.2}Mo_{0.8}$ | 4.6 | γ-$Bi_2Mo_1O_6$, β-$Bi_2Mo_2O_9$ | 131.2 | 1.00 | 0.19 | 0.69 | 5.6 | 16.5 | 79.0 | 0.9 |
| $BiV_{0.4}Mo_{0.6}$ | 2.4 | $Bi_{0.88}Mo_{0.37}V_{0.63}O_4$, γ-$Bi_2Mo_1O_6$ | 194.5 | 1.00 | 0.45 | 0.55 | 65.3 | 89.1 | 9.0 | 58.2 |
| $BiV_{0.6}Mo_{0.4}$ | 2.5 | $Bi_{0.93}Mo_{0.21}V_{0.79}O_4$, γ-$Bi_2Mo_1O_6$ | 225.3 | 1.00 | 0.58 | 0.40 | 72.2 | 88.6 | 9.9 | 64.0 |
| $BiV_{0.8}Mo_{0.2}$ | 2.6 | $Bi_{0.93}Mo_{0.21}V_{0.79}O_4$, γ-$Bi_2Mo_1O_6$ | 163.4 | 1.00 | 0.78 | 0.12 | 23.2 | 41.0 | 55.3 | 9.5 |
| BiV | 0.9 | $BiVO_4$ | 94.5 | 1.00 | 0.91 | - | 0.6 | 7.7 | 90.1 | 0.0 |

[a] Determined by $O_2$-pulse experiments.

[b] Determined from ICP-AES.

[c] The conversion and selectivity were obtained after an 8 h ODH reaction. Reaction conditions: 0.5 g catalyst, T = 420 $^oC$, 1–$C_4H_8$/air/$H_2O$ = 1/3.75/5 and total flow rate = 78 $cm^3$ $min^{-1}$.

ACCEPTED MANUSCRIPT

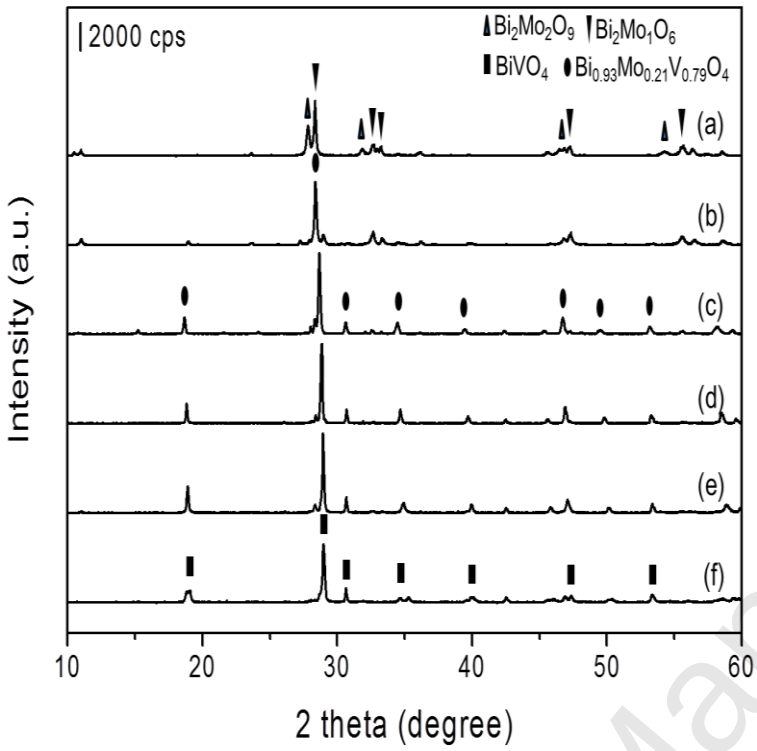


Fig. 1

Accepted Manuscript

ACCEPTED MANUSCRIPT

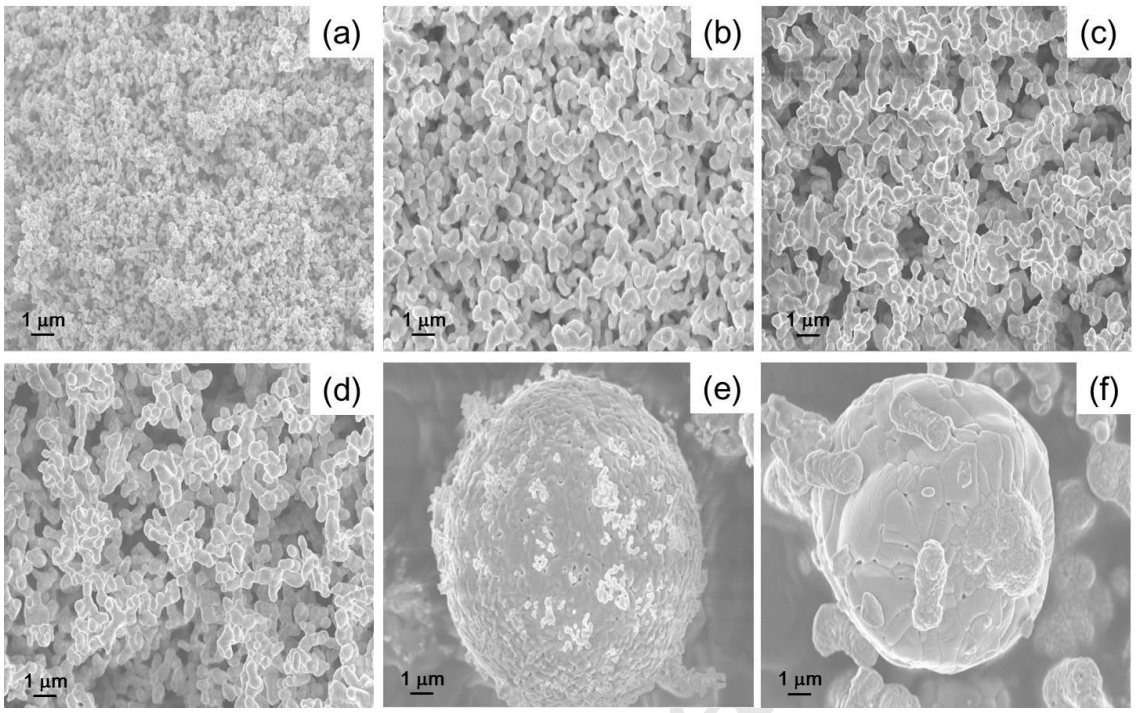


Fig. 2

Accepted Manuscript

ACCEPTED MANUSCRIPT

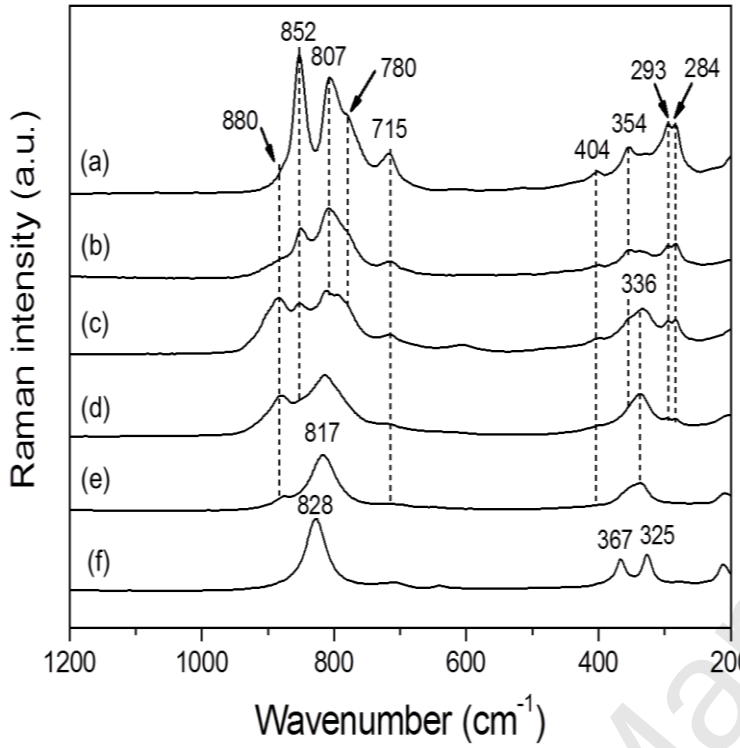


Fig. 3

Accepted Manuscript

ACCEPTED MANUSCRIPT

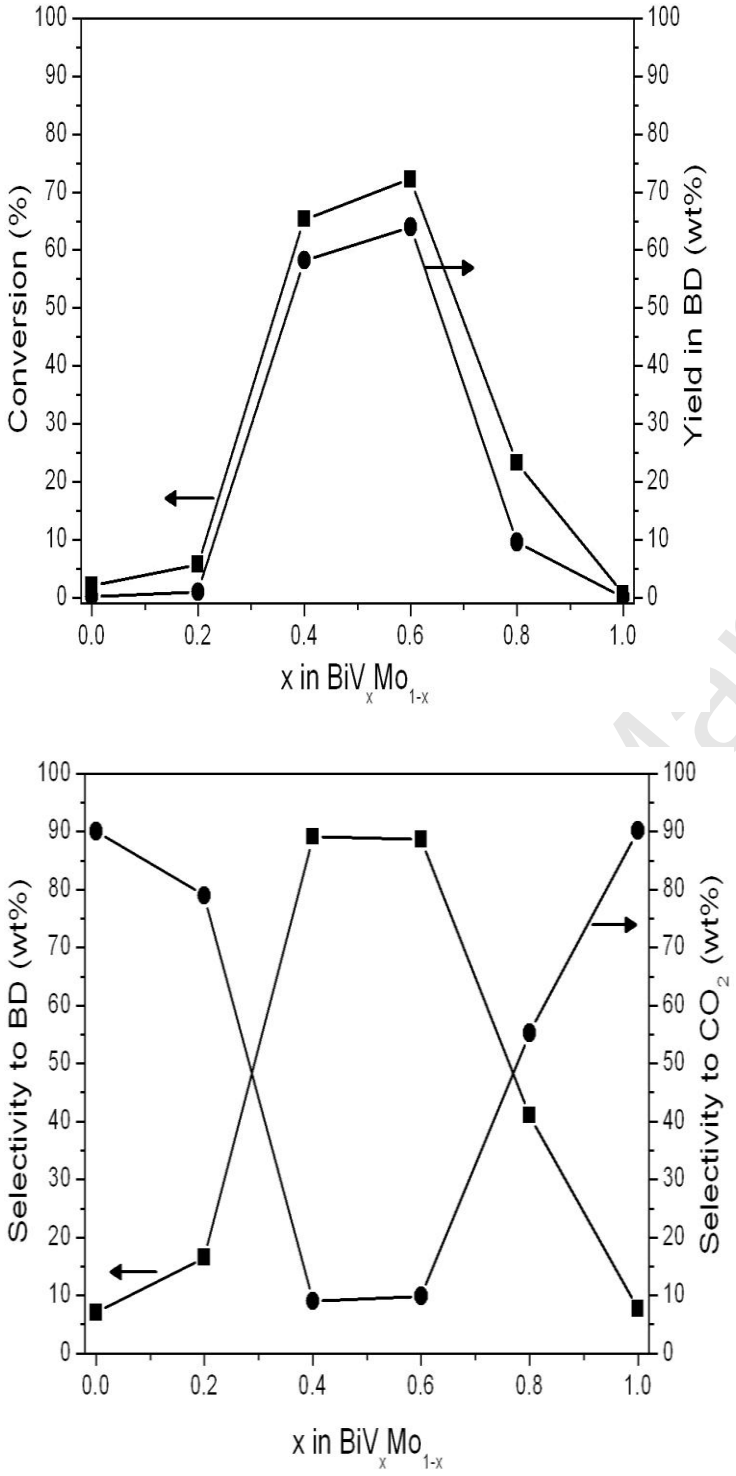


Fig. 4

ACCEPTED MANUSCRIPT

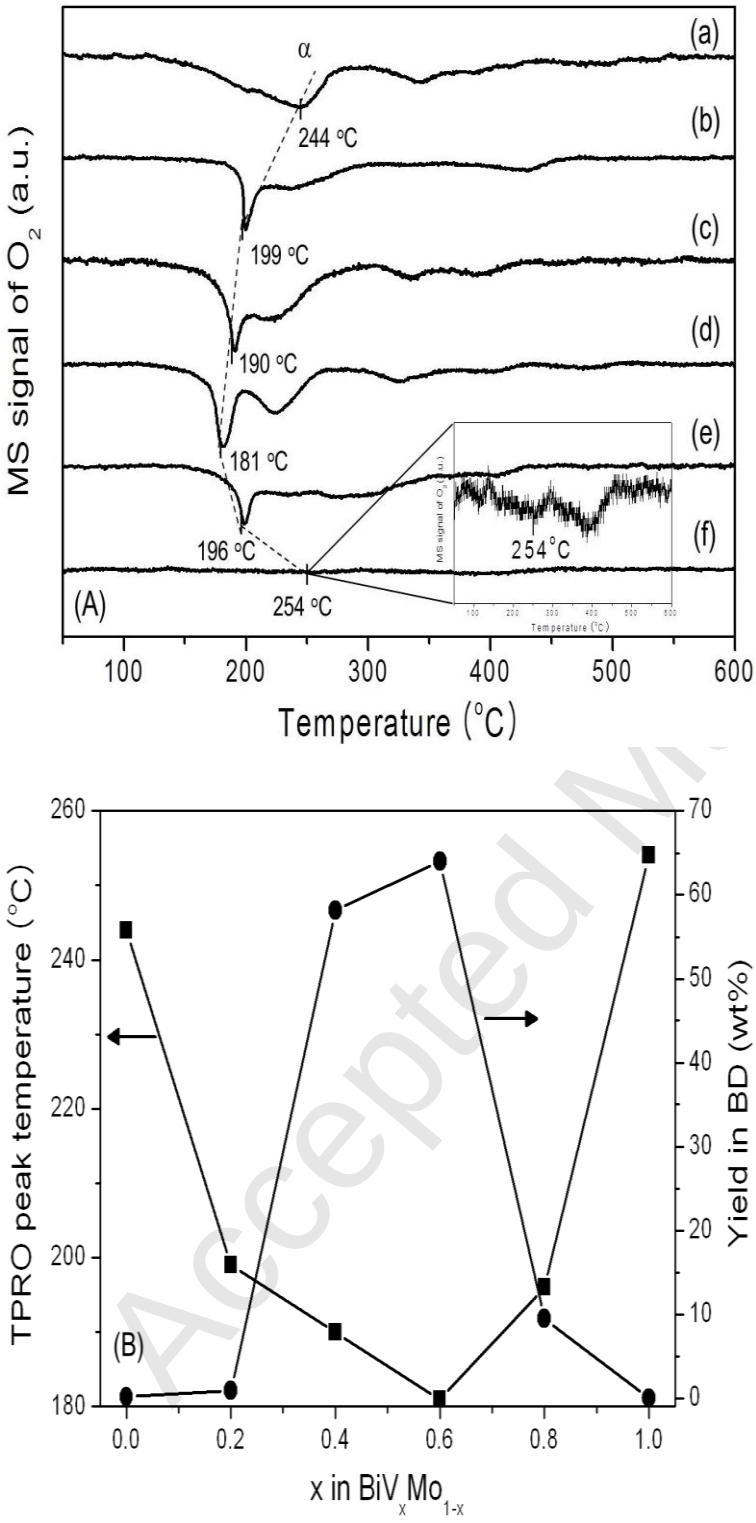


Fig. 5

ACCEPTED MANUSCRIPT

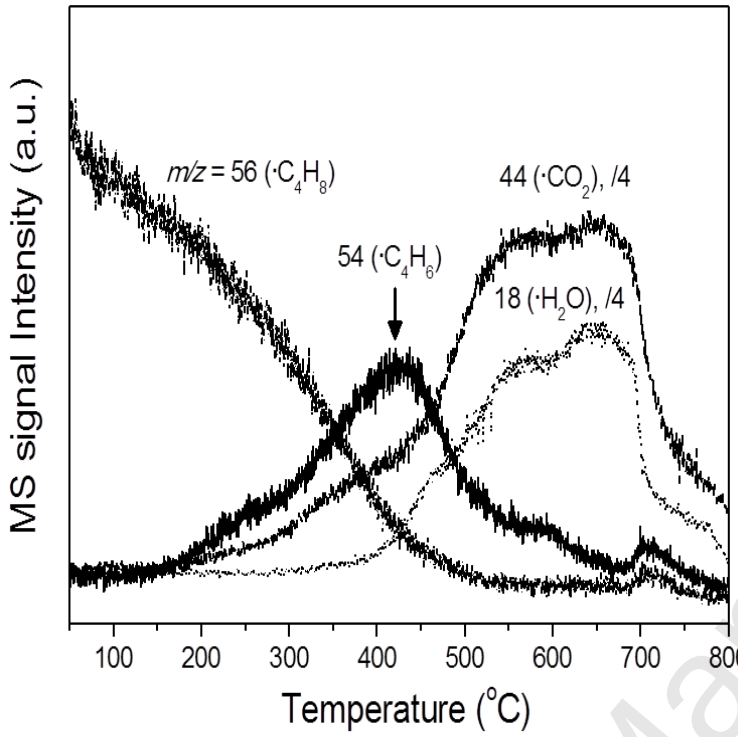


Fig. 6.

Accepted Manuscript

ACCEPTED MANUSCRIPT

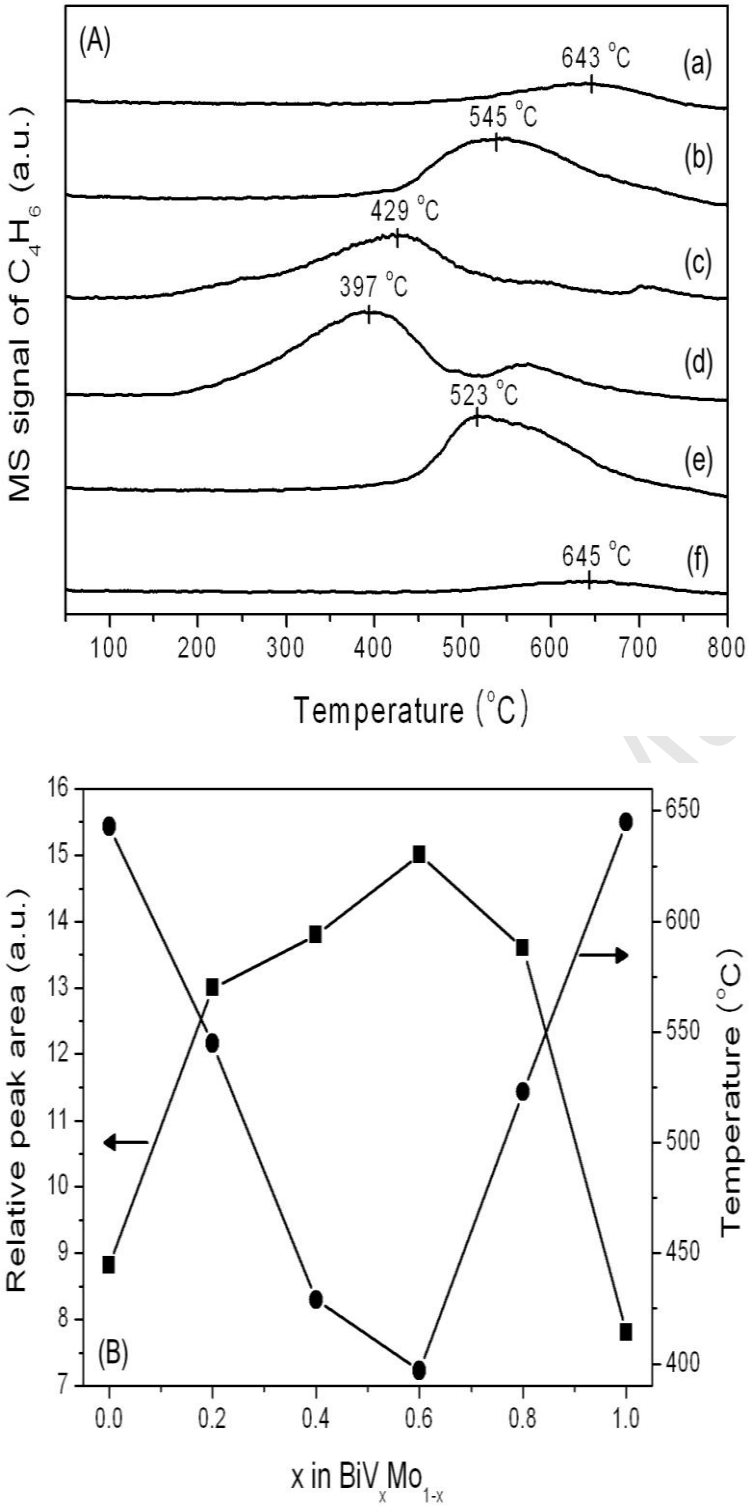


Fig. 7

ACCEPTED MANUSCRIPT

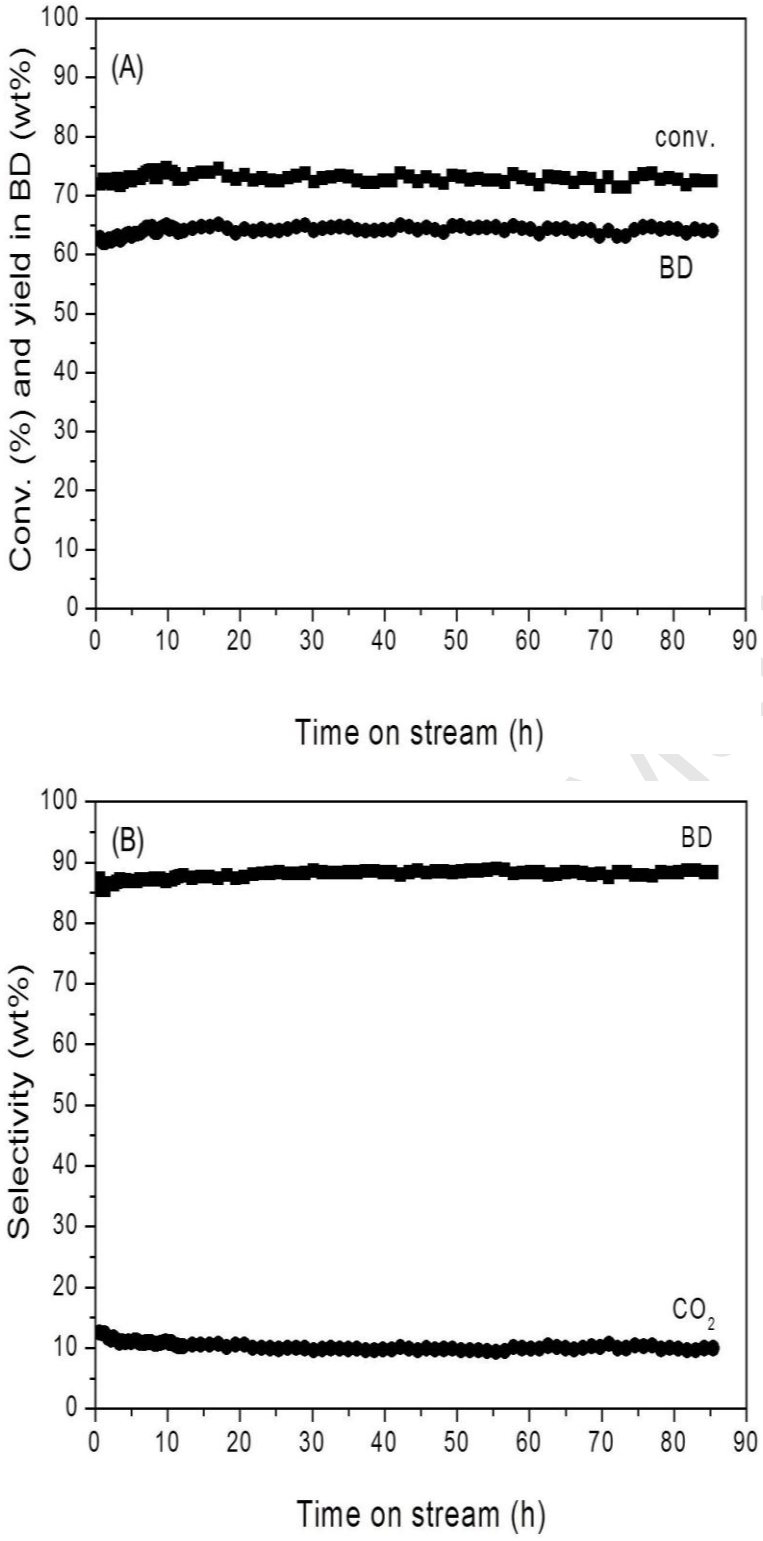


Fig. 8